

# Thermodynamics of gold nanoparticle growth: A first-principles investigation

Thesis for the degree of Erasmus Mundus  
Master of Science in Nanoscience and Nanotechnology

**HIMANSHU SHEKHAR**  
Department of Applied Physics,  
CHALMERS UNIVERSITY OF TECHNOLOGY,  
GÖTEBORG, SWEDEN 2013



**CHALMERS**

---

Thesis for the degree of Erasmus Mundus  
Master of Science in Nanoscience and Nanotechnology

# Thermodynamics of gold nanoparticle growth: A first-principles investigation

**Supervisor:**

Paul Erhart, Chalmers University of Technology, Sweden

**Co-supervisor:**

Steven De Feyter, K U Leuven, Belgium

**External examiner:**

Kasper Moth-Poulsen, Chalmers University of Technology, Sweden



**CHALMERS**

Department of Applied Physics,  
CHALMERS UNIVERSITY OF TECHNOLOGY  
Göteborg, Sweden 2013

This master thesis is conducted in the framework of Erasmus Mundus Master  
Programme in Nanoscience and Nanotechnology

---

**Thermodynamics of gold nanoparticle growth:  
A first-principles investigation**

Himanshu Shekhar

©Himanshu Shekhar, 2013

Department of Applied Physics,  
CHALMERS UNIVERSITY OF TECHNOLOGY  
SE 412-96, Göteborg, Sweden 2013

Printed by Chalmers reproservice  
Göteborg, Sweden 2013

## Abstract

Good control over size and shapes of nanoparticles is key for their usage as basic building blocks in various applications. Nanocrystals are of immense interest because of their electronic, optical, and magnetic properties, which are dependent on size and morphology of the nanocrystals. Hence by controlling these parameters it is possible to tune these properties as well. In spite of significant progress in the area of crystallography and materials science the underlying growth mechanism of anisotropic nanocrystals has not been resolved to a satisfactory level. Proper understanding of growth and control mechanism is key for further improvement, which will open the door for applications in new areas.

Gold nanorods are examples for anisotropic nanocrystals which is a topic of research for many groups. Bottom-up, e.g., templating, electrochemical and top-down, e.g., photolithography are two methods for the synthesis of metal nanoparticles. One of the most widely used methods for the synthesis of anisotropic gold nanorods is surfactant assisted seed mediated growth from solution. Seed mediated growth is a wet chemical method is a cheap and easy process. While it offers several advantages over electrochemical processes, it suffers from low yield and the unpredictable morphology of the end product in many cases.

The objective of this thesis is to resolve the thermodynamics of the growth of Au nanoparticles and rods using cetyltrimethylammonium bromide as growth agent. To this end the surface energetics of a variety of different Au surfaces with and without surfactant are obtained using electronic structure calculations based on density functional theory. The results are discussed in the context of experimental observations. The growth of nanocrystals is not an equilibrium phenomena so its growth mechanism cannot be explained by pure thermodynamics alone. The present study provides basic thermodynamic parameters, which determine the driving forces and exact knowledge of which is a prerequisite for understanding the non-equilibrium growth process. Thereby present work lays the ground for future studies that should address, for example, entropic and kinetic factors in order to get a comprehensive picture of nanocrystal and nanorod formation.

## Acknowledgements

The work presented in this thesis was carried out at the Applied Physics department at Chalmers University, in the year 2013. It is now my responsibility and pleasure to express my gratitude to the people involved in this work.

I greatly acknowledge my supervisor Asst. Prof. Paul Erhart for accepting me for this master thesis project. Paul's trust, patience, and knowledge made this journey possible. I am grateful to Prof. Steven De Feyter for co-supervising me. I am grateful to Asst. Prof. Kasper Moth-Poulsen for first introducing me to this project and later for accepting the role of referee in my thesis defense.

I recognize the help of all PhD students of Materials and Surface theory group at Chalmers university. I would also like to thank my program coordinators Prof. Guido Groenseneken and Prof. Göran Johansson for their roles. Finally, I would like to thank my EMM Nano classmates with whom I spent a great time of my life during this master program.

# Contents

<b>1</b>	<b>Introduction</b>	<b>1</b>
1.1	Background . . . . .	1
1.2	Scope and Outline . . . . .	3
<b>2</b>	<b>Methodology</b>	<b>5</b>
2.1	Density Functional Theory . . . . .	6
2.2	Exchange-Correlation Functional . . . . .	7
2.3	Choice of Basis Set . . . . .	8
2.4	Pseudopotentials . . . . .	10
2.5	Brillouin Zone Integration . . . . .	10
2.6	Slab Models of Surfaces . . . . .	11
2.7	Computational Setup . . . . .	12
<b>3</b>	<b>Thermodynamics</b>	<b>13</b>
3.1	Thermodynamics versus Kinetics . . . . .	13
3.2	Thermodynamic Driving Forces . . . . .	15
3.3	Surface Free Energy . . . . .	16
3.4	Thermodynamics of Adsorption . . . . .	17
3.4.1	Adsorbates . . . . .	17
3.4.2	Approximations . . . . .	18
3.4.3	Adsorption Sites . . . . .	19
3.5	Coverage . . . . .	20
3.6	Equilibrium Shape . . . . .	21
<b>4</b>	<b>Results and Discussion</b>	<b>23</b>
4.1	Adsorption . . . . .	23
4.1.1	Adsorption Sites . . . . .	23
4.1.2	Br on Low Index Au Surfaces . . . . .	23
4.1.3	BTA <sup>+</sup> on Low Index Au Surfaces . . . . .	25
4.1.4	BTAB on Low Index Surfaces . . . . .	26
4.1.5	Br on High Index Surface . . . . .	28

4.1.6	BTA <sup>+</sup> on High Index Surface . . . . .	28
4.1.7	BTAB on High Index Surface . . . . .	29
4.2	Surface Energy . . . . .	31
4.2.1	Surface Energies of Clean Au Surfaces . . . . .	31
4.2.2	Surface Energies Change due to Adsorption . . . . .	31
4.3	Equilibrium Crystal Shape . . . . .	35
<b>5</b>	<b>Discussion and Conclusion</b>	<b>41</b>
5.1	Template Assisted Growth . . . . .	41
5.1.1	Chemical Potential . . . . .	41
5.1.2	Anisotropic Shapes and Symmetry Breaking . . . . .	42
5.2	Conclusion . . . . .	44
	<b>Bibliography</b>	<b>47</b>

# Chapter 1

## Introduction

### 1.1 Background

Most of us must have seen ice, a form of crystal, in various sizes and shapes. Why do they form from liquid? Why do they grow in different shapes? Why does a flake of ice grow differently on a surface of water in a pond than the one in our freezer? The first question is not difficult to answer. Ice grows from liquid because it lowers its free energy by doing so. The second question is, however, not so easy to answer. One can make an educated guess that it, probably temperature, the surface on which the ice grows, and the environment which dictate the final shapes of ice flakes. The details, however, are as usual more complicated.



**Figure 1.1:** (a) Calcidiscus, a biomineralized crystalline product (from the International Nanoplankton Association website). (b) Nano-Flower, a germanium-sulfide nanosheet structure (from the Materials Research Society).

An intriguing branch of materials science is concerned with resolving the growth mechanism of organic and inorganic nanocrystals. It is interesting to



know that humans are not the first species, which envisaged the potential application of nanocrystals. Many living organisms in nature use biomineralization processes to build shells such as these shown in Fig. 1.1(a) and many other patterned structures. These organisms are able to control nucleation, crystal shape, and material structure. What is most striking is the degree to which these organisms are able to control the growth of crystallites and the crystallographic orientation of its functional material compared to synthetically produced crystals.

Taking a cue from this beautiful work of nature there have been continuous efforts see Fig. 1.1(b), to imitate it in the laboratory for its potential application in fields of electronics, bioimaging, biosensing, and optics. Gold nanorods are of particular interest for their potential use in biosensing and bioimaging mainly because of the inertness of gold metal in biological environments [1]. In spite of the enormous success in growing nanocrystallites and nanorods of various shapes the details of the growth process are still incompletely understood. A good example is surfactant assisted seed mediated growth of nanorods [2, 3, 4, 5], which also is the subject of this thesis. Several research groups have adopted the seed mediated approach in aqueous solution using cetyltrimethylammonium bromide (CTAB) as surfactant to produce gold nanorods.

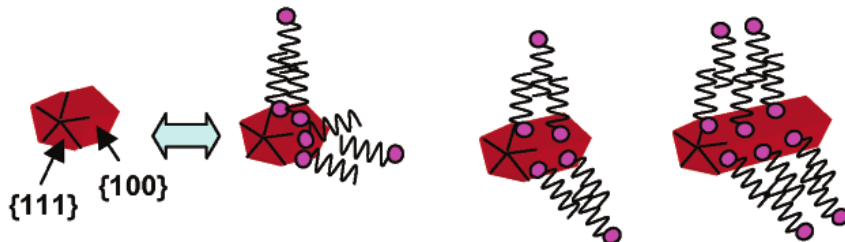


**Figure 1.2:** Growth of gold nanorods using CTAB bilayer as template. Binding of CTAB to Au (100) facet and growth along (111) [2].

There is, however, still ambiguity when it comes to describing the growth mechanism. The role of surfactants is not clearly known. The general tendency in the literature is to emphasize the role of surfactants as shape directing agent. First Nikkobakht and later Murphy and co-workers proposed a zipping mechanism [6, 2], Fig. 1.2, for nanorod like growth. In the zipping mechanism the surfactants starts forming a bilayer in the solution at the critical micelle concentration. These bilayers act like a template on which incoming monomers attach and form a rod like shape. Others [7] argued that a bilayer structure formation is not necessary for the growth of nanorods. The surfactants are normally bigger in size compared to the monomer units of crystals thus steric effects are also important. While surfactants thus definitely play an impor-

tant role in the growth of anisotropic nanocrystals, the exact role they play is largely unknown.

## 1.2 Scope and Outline

The objective of this thesis is to resolve the thermodynamics of growth of gold nanoparticles and predict their equilibrium shape under different conditions. All calculations in this work are based on the assumption that the nanocrystallite is in equilibrium with the surrounding medium. We are only concerned with the surface and neglect any bulk effects such as strain. We have also neglected corner and edge effects.

The first step towards achieving this goal is to find a set of computational parameters that ensure numerically converged calculations. Using the thus determined parameters the surface free energies of bare gold surfaces are computed to establish their relative stability. Motivated by the structural information on gold nanorods available in the literature [8, 9, 5], several surfaces of face centered cubic (FCC) gold crystal have been considered in this project. Surfactants change the surface free energy. Here we consider butyltrimethylammonium bromide (BTAB) as a surrogate for CTAB. After finding the equilibrium positions the surface energy is calculated at different surface coverages. The thus obtained surface energies are then being used to predict equilibrium shapes using the Wulffconstruction method.

All computations are done within density functional theory (DFT) [10] using the projector augmented wave method as implemented in vienna ab-initio simulation package [11]. Chapter 2 will discuss basics of DFT with some comments on its accuracy in the present context. Chapter 3 is devoted to thermodynamics, its influence on gold nanorod growth and on the equilibrium shape of nanocrystallites. Results are compiled in chapter 4 and finally this thesis concludes with discussion and some final remarks.



# Chapter 2

## Methodology

To calculate the structure and electronic properties of molecules and solids requires solving the Schrödinger equation. For most systems it is impossible to solve the quantum many-body problem analytically. A number of numerical techniques have been formulated to solve such problems. These techniques include methods such as hartree-fock, quantum monte carlo [12], density functional theory [10]. The primary purpose of any *ab-initio* calculation is to characterize a material without any experimental or empirical input. Atomic positions and atomic numbers are in principle the sole input parameters in these methods. With recent developments in theoretical techniques and the continuous increase in computational power, *ab-initio* techniques are not only limited to the structural study of materials but also being used for example in the study of defects in materials, adsorption on surfaces, and other surface related phenomena. *Ab-initio* calculations not just give information about the ideal state of a system but can also help understand the impact of temperature, pressure, and chemical composition. These studies have helped our understanding of new materials and lead to further insights and predictions, which would be nearly impossible to achieve experimentally.

The following sections provide a brief overview of density functional theory (DFT) and its practical aspects, such as pseudopotentials, exchange-correlation functionals, and Brillouin-zone sampling. We also introduce the slab model of the gold surface, which will be our basic platform for all subsequent computations. We then finish the chapter by describing the periodic superstructure of adsorbates on gold surfaces.

## 2.1 Density Functional Theory

The objective of DFT is to obtain ground state properties of any system in an external potential. DFT is based on set of approximations, which simplify the original many body time independent Schrödinger equation,

$$\left[ \frac{-\hbar^2}{2m} \sum_{i=1}^N \nabla^2 + \sum_{i=1}^N V(r_i) + \sum_{i=1}^N \sum_{j<i} U(r_i, r_j) \right] \psi = E\psi, \quad (2.1)$$

where the first term on the left side represents the kinetic energy, the second term is the interaction between electrons and the external potential, and the third term corresponds to the interaction between electrons.

The Hamiltonian depends on the spatial coordinates,  $r_i$ , of each electron in the system. It represents a formidable task to solve above equation numerically even for a small number of electrons. A breakthrough came in the mid 1960ies when Hohenberg and Kohn [13] proved that the energy of a system is a unique functional of the electron density

$$E = F[n(r)], \quad (2.2)$$

where  $E$  is the energy and  $n(r)$  is the ground state electron density. The second theorem states that the electron density, which minimizes the ground state energy, is the true ground state electron density.

Kohn and Sham [14] later showed that the problem can be expressed as a set of single particle equations,

$$\left[ -\frac{\hbar^2}{2m} + V_{ion}(r) + V_H(r) + V_{XC}(r) \right] \psi_i(r) = \varepsilon_i \psi_i(r), \quad (2.3)$$

where the first term on the left hand side again represents the kinetic energy. The second term corresponds to the external potential, the third term is the Hartree potential and the last term is the so-called exchange-correlation potential.

The Kohn-Sham formulation transforms the fully interacting many-body problem given by (2.1) into a non-interacting system, where each electron moves within an effective potential. The problem posed by (2.3) is solved numerically in a self-consistent way as follows

1. An initial trial electron density  $n(r)$  is generated, usually by superposition of atomic densities.
2. Using  $n(r)$  the effective potential (expression in the brackets on the left hand side of (2.3)) is evaluated

3. The Kohn-Sham equation (2.3) is solved to get the single particle wave functions  $\psi_i(r)$ .
4. The thus obtained wave functions are used to calculate the electron density as  $n(r) = \sum_i \psi_i^*(r)\psi_i(r)k_i k_i$  is the occupation
5. The new electron density is compared with the approximated electron density. If the two densities are the same then this is the true ground state electron density. If the two electron densities differ, the density is updated and the cycle is repeated.

It is still a formidable task to solve the above problem numerically. A host of algorithms has been developed to accomplish steps 1-5 as efficiently as possible [10, 12].

## 2.2 Exchange-Correlation Functional

The exact form of the exchange-correlation potential  $V_{XC}(r)$ , which can be expressed as a functional derivative of the exchange-correlation energy,

$$V_{XC}(r) = \frac{\delta E_{XC}(r)}{\delta n(r)}, \quad (2.4)$$

is unknown. Over the course of time several exchange-correlation functionals, including for example local density (LDA), and generalized gradient approximations (GGA), have been formulated to study different kind of systems and to achieve maximum chemical accuracy. The simplest approximation is the LDA, which is derived from the homogeneous electron gas. The local density approximation for the exchange correlation energy is written as

$$E_{XC}^{\text{LDA}}[n(r)] = \int n(\mathbf{r})\varepsilon[n(\mathbf{r})]d\mathbf{r} \quad (2.5)$$

where  $n(\mathbf{r})$  is the electron density and  $\varepsilon[n(\mathbf{r})]$  is the exchange-correlation energy density.

One might ask whether the LDA a good choice for all systems! For bulk material this might be a choice but for atoms, molecules, and interfaces where the electron density has large gradients a different exchange-correlation potential is required. LDA are important in the construction of more sophisticated functionals, such as GGA or hybrid functionals. In the study of systems where the electron density is not uniform, the exchange-correlation functional can

be represented as a GGA, which takes into account the spatial variation of the electron density in the system

$$E_{XC}^{GGA}[n(r)] = \int n(r)\varepsilon[n(r), \nabla n(r)]dr \quad (2.6)$$

where  $n(r)$  is the electron density and  $\nabla n(r)$  is its gradient.

There is a large family of GGA functionals. In this work all calculations are performed using the generalized gradient approximation as parameterized by Perdew-Burke-Ernzerhof (PBE) [15].

## 2.3 Choice of Basis Set

Our objective is to solve the single particle Kohn-Sham equations, (2.3). This requires to define a basis set, in which the one particle orbitals  $\phi_{\mathbf{k}}(\mathbf{r})$  are represented. Some possible basis sets include linear combination of atomic orbitals, real space grid, and plane waves. Plane waves are a good choice for periodic systems and therefore also a good option for our systems. Plane waves have the advantage that they are numerically very efficient since transformation from real to reciprocal space are fast. We can express the single particle wave functions as

$$\phi_{\mathbf{k}}(\mathbf{r}) = \exp(i\mathbf{k} \cdot \mathbf{r})u_{\mathbf{k}}(\mathbf{r}) \quad (2.7)$$

where  $\exp(i\mathbf{k} \cdot \mathbf{r})$  is a plane wave function with wave vector  $\mathbf{k}$ , and  $u_{\mathbf{k}}(\mathbf{r})$  is a Bloch function with the same periodicity as the supercell. The periodicity of  $u_{\mathbf{k}}(\mathbf{r})$  means that the single particle wavefunction can be expanded in plane waves as

$$\phi_{\mathbf{k}}(\mathbf{r}) = \sum_G c_G \exp(i(\mathbf{k} + \mathbf{G}) \cdot \mathbf{r}) \quad (2.8)$$

where the coefficient  $c_G$  is the probability amplitude corresponding to each basis function and  $G$  is a reciprocal lattice vector. According to this expression evaluation of  $G$  involves a summation over an infinite number of values of  $G$  in the reciprocal space, which has to be cutoff for practical computations. It is common to set a cutoff for the value of  $G$  based on the maximum kinetic energy of any of the plane waves is,

$$E_{\text{cutoff}} = [\hbar^2/2m]G_{\text{cut}}^2 \quad (2.9)$$

The infinite sum in Eq. (2.8) then becomes

$$\phi_{\mathbf{k}}(\mathbf{r}) = \sum_G^{G_{\text{cut}}} c_G \exp[i(\mathbf{k} + \mathbf{G}) \cdot \mathbf{r}] \quad (2.10)$$

We have thus introduced a new parameter, the cutoff energy  $E_{cut}$ , which must be defined in a DFT computation. The cutoff energy is element specific so care needs to be taken when dealing with multi element system. Generally the largest cutoff energy for any of the element in the system is taken as the cutoff energy for the compound system as demonstrated by the following example. Consider an arbitrary adsorbate on a surface e.g., CTAB on a gold surface. A supercell of this system contains Au, C, N, Br, and H, for which the plane wave energy cutoff are given in table below. For this computation the energy cutoff value should thus be at least 300 eV.

**Table 2.1:** Plane wave energy cutoff energies of elements in a compound system.

Element	$E_{max-cut}$ (eV)	$E_{min-cut}$ (eV)
Au	230	172
C	400	300
N	400	300
H	250	200
Br	216	162

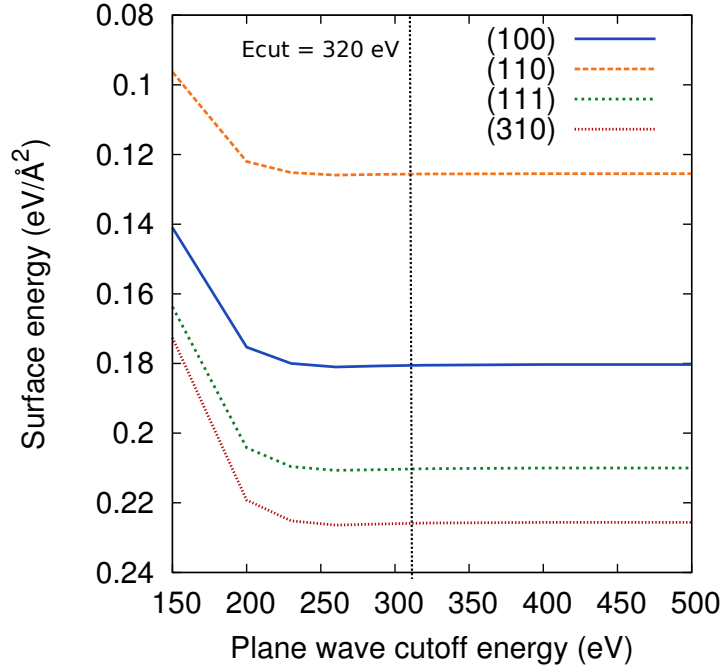


**Figure 2.1:** Convergence with plane wave cutoff energy.

In practice the plane wave cutoff energy (just as any of the other numerical



parameters e.g., number of  $k$ -points) should be chosen such that the property of interest, e.g., lattice constant, surface energy or the total energy of the system are converged to the desired accuracy. Figure 2.1 shows the convergence of the surface energy with the plane wave energy cutoff. It demonstrates that a cutoff energy of at least 300 eV is required to converge the surface energies. It also shows that energy differences converge faster than total energies.

## 2.4 Pseudopotentials

In the description of the basis set, we did not mention valence and core electrons and also we did not discuss the description of the wave function in the vicinity of the nucleus. The tightly bound core electrons have wave functions that oscillate rapidly close to the nucleus. A large cutoff energy is needed to make the wave function smooth. A large cutoff energy means a large number of plane wave components, which is computationally very cumbersome. To reduce the burden, pseudopotentials are used, which basically replaces core electrons with a smooth potential. This approximation is justified because from a physical point of view, it is the valence electrons that are important in a reaction. In this thesis work, all DFT computations are done using the projector augmented wave method [16, 11], which represents a generalized version of the pseudopotential method and also a connection to the linear augmented plane wave method.

## 2.5 Brillouin Zone Integration

The observables, energy and electron density, of the Kohn-Sham equation (2.3) are calculated by integrating over the first Brillouin zone (BZ). A great deal of work reduces to evaluating integrals of the form

$$E_{total} = \frac{1}{V_{BZ}} \int_{BZ} E(\mathbf{k}) d\mathbf{k} \quad (2.11)$$

where  $E_{total}$  is the energy of the ground state and  $V_{BZ}$  is the volume of the BZ. The integral in Eq. (2.11) is defined in reciprocal space and integrated over all possible  $\mathbf{k}$  values. Numerically this integration is done by replacing the integral with a summation over a discrete set of  $\mathbf{k}$  points as described below.

The integral of the function shown in Fig 2.2 is the area under the curve that is found by integrating in the interval  $[-\frac{\pi}{L}, \frac{\pi}{L}]$ . A simple way to approximate this integral is to break up the interval into equal pieces and estimate the area using the trapezoidal method.

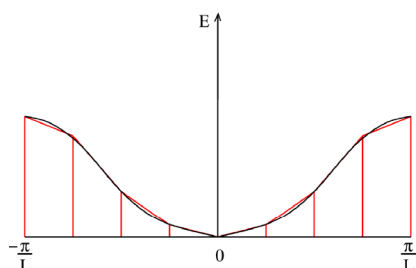


Figure 2.2: Numerically integrating over Brillouin zone

The  $k$ -point grid used in DFT calculations is dependent on several factors, such as type of material, size of supercell<sup>1</sup>, crystal structure, etc. A metal requires a different number of  $k$ -points than a semiconductor or an insulator because of the difference in the Fermi surface. Another example is the size of the supercell as a small supercell in real space corresponds to a large volume in reciprocal space and vice versa. By keeping these things in mind one can save lots of computational time without compromising the result.

## 2.6 Slab Models of Surfaces

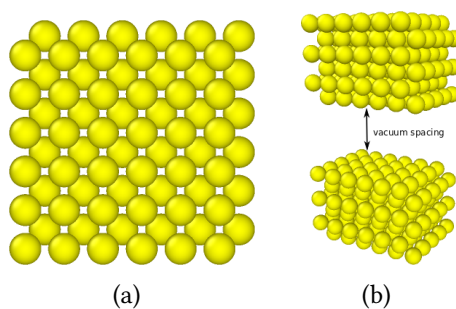


Figure 2.3: (a) Slab model of (100) surface of Au crystal. (b) Vacuum spacing between two neighbouring slabs.

Crystallites are microscopic crystals bound by several facets. Facets in nanocrystals are flat surfaces, which appear during crystal growth. Thus it is vital to start our study with the surface of the crystal. To represent surfaces in our DFT study we analyzed slab models, Fig. 2.3(a). These models are computationally efficient as they are infinite in two dimensions due to application

<sup>1</sup>cell that contains more than one primitive cell

of periodic boundary condition, but finite in the third and yet have all the properties of a real surface. Along the vertical direction slabs are separated from each other by a minimum distance to avoid any kind of interaction between them. The spacing, denoted as vacuum space in Fig 2.3 (b), varies with the type of adsorbates on the surface. For example, an adsorbate with a long tail would require a larger vacuum spacing because electrons in the chain would be closer to the next slab.

## 2.7 Computational Setup

In this thesis work, we have used python and the atomic simulation environment (ASE)[17] to construct the atomistic system. Another tool, which has been used quite extensively in this thesis work, is Ovito [18]. Ovito is a visualization tool for atomistic models that proved very handy in the analysis of structures.

All DFT calculations are performed using the projector augmented wave method [16] as implemented in the Vienna *ab-initio* simulation package VASP [11]. The exchange-correlation potential used in our DFT calculation is Perdew, Burke, and Ernzerhof (PBE) and is based on the generalized gradient approximation.

In all the calculations involving Au and the adsorbate butyltrimethylammonium bromide (BTAB), a plane wave cut-off energy of 320 eV was used. For comparison also calculations with a cutoff energy of 500 eV were carried out. The difference in the adsorption energy of the system with respect to a cutoff energy at 320 eV is around 9 meV which is less than  $kT$  value at room temperature.

Surfaces with several different orientations were considered. The slab models for (100), (110), and (111) contain 10 atomic layers whereas in the case of (310), 6 atomic layers were considered. A vacuum spacing of 12 Å was used in all computations.

# Chapter 3

## Thermodynamics

### 3.1 Thermodynamics versus Kinetics

The whole of Materials and Surface science can be represented as a battle between thermodynamics and kinetics. This battle is driven by the driving forces and the energy barriers of the landscape. Thermodynamics tells whether a certain transformation is favourable or not, i.e., if there is a decrease in the free energy or not. It gives an account of driving forces required for a reaction to occur. Kinetics is all about, how fast or slow a process can occur i.e., determines the rate. The kinetics of a reaction is about how to overcome energy barriers and reach the final state.

The way in which kinetics affect the rate of transformation can be understood from Fig. 3.1. The final state is lower in energy than the initial state. It means that the system gains free energy by changing its state from initial to final. This difference in the free energy  $\Delta G$  is the thermodynamic driving force. However, the barrier, which a particle must cross in order to reach to the final state, requires energy from thermal activation. The particle must have energy equal to the activation energy in order to cross it. A particle in an ensemble gains energy by random collisions with other particles and at some point of time it will gain enough energy to overcome the barrier. This transformation rate can be written down as

$$R = A \exp \left[ -\frac{E}{kT} \right], \quad (3.1)$$

where  $E$  is the activation barrier,  $k$  is the Boltzmann constant,  $T$  is temperature and  $A$  is a pre-factor. The larger the barrier, the more difficult the process to occur, the slower the rate. Thus by varying the heights of the energy barriers, the transformation rate can be controlled. In short, thermodynamics tells us

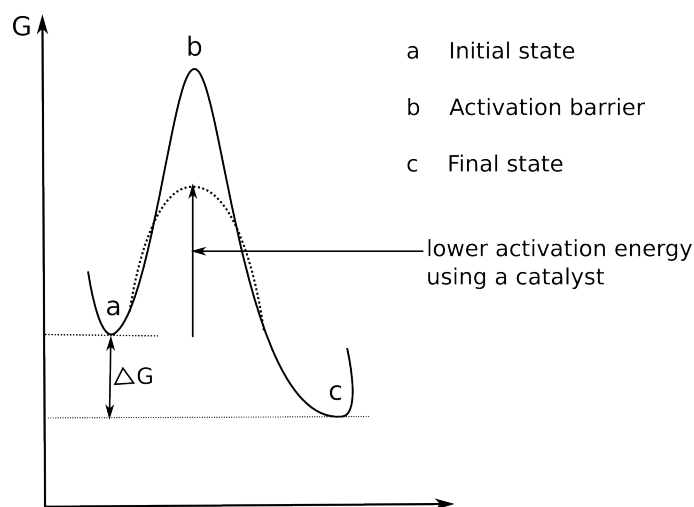


**Figure 3.1:** Transition from initial state (a) to final state (c) through an activation state (b). Energy barrier is modified when catalyst is used in the reaction.

that a reaction or transformation should take place if the final product is more stable than the initial state. Kinetics concerns the rate of transformation.

A process concerned with kinetics could be a simple chemical reaction, or a transformation from one phase to another. Crystallization, the process by which crystals form from solution or from vapour, is a field that is very much concerned with kinetics. The shape of crystals is highly influenced by kinetic factors, such as diffusion, adsorption, and desorption. One of the major difficulties in understanding the growth mechanism of crystals is the complexity of the energy landscape.

A very generalized picture of a crystal's physical and energy landscape is shown in Fig. 3.2. An incoming adatom randomly occupies a site on the crystal surface. This adatom however, does not remain there for long as it hops between sites and in the process occupies another sites that must be lower in energy. The particle gets energy for hopping from thermal agitation and frequent collision with other particles and gradually moves from one state to the another state. The different energy barriers along the migration path of the adatom determine the time scale of transformation. There are many examples in nature, which are thermodynamically favourable but kinetically unfavourable. Graphite and diamond are both forms of carbon, but graphite has a lower free energy than diamond. Thermodynamically, transformation from diamond to graphite is favourable. It is, however, kinetically hindered because the transition states are so high in energy that the transition rate is extremely small.

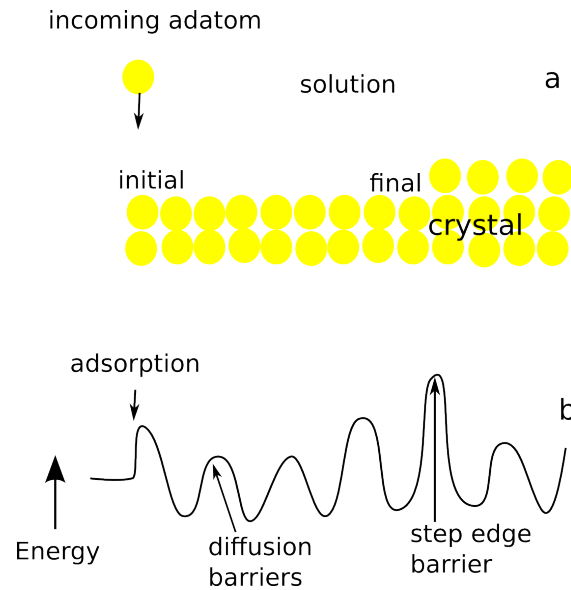


**Figure 3.2:** Schematic of (a) physical and (b) energy landscape of a surface with one adatom.

## 3.2 Thermodynamic Driving Forces

So what drives a phase transformation? Phase transformation takes the system to a new state whose free energy is different from the initial state. This change in free energy provides the necessary driving force. Gibbs free energy comprises contributions from the enthalpy and the entropy of the system. It is defined as

$$G = E + pV - TS, \quad (3.2)$$

where  $G$  is Gibbs free energy,  $E$  the internal energy of the system,  $p$  the pressure,  $V$  the volume,  $T$  the temperature, and  $S$  the entropy of the system. The  $E + pV$  term is the enthalpy  $H$  of the system

$$G = H - TS. \quad (3.3)$$

Figure 3.3(a) shows a liquid-solid system in equilibrium at the melting temperature  $T_m$ . The thermodynamic driving force in this case is  $\Delta G = 0$ . It means the net transfer of number of particles across the interface is zero. Figure 3.3(b) is the same liquid-solid system but under a finite driving force, which arises for example if  $T$  is slightly lower than  $T_m$ . In the second case there exists a driving force  $\Delta G = G_S - G_L < 0$ , which favours the transformation. This driving force is dependent on thermodynamic parameters, such as temperature, pressure, composition, etc. Thus by varying these parameters it is possible to manipulate the driving force.

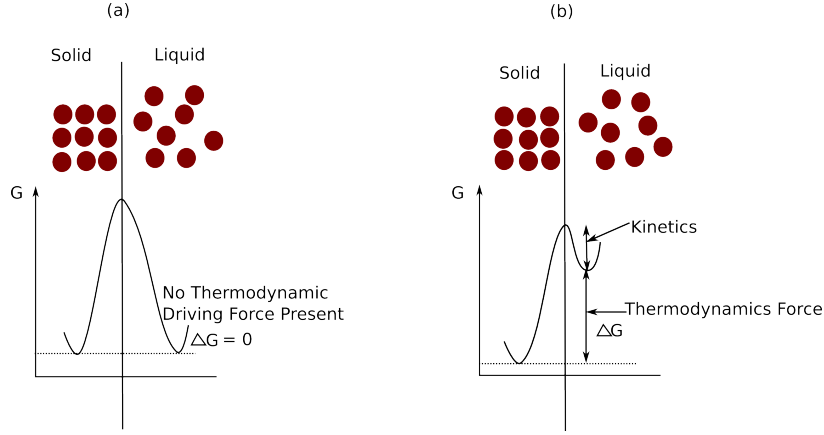


**Figure 3.3:** Liquid-crystal interface (a) at equilibrium and (b) subjected to a finite driving force.

### 3.3 Surface Free Energy

The surface energy measures the energy needed to break a bulk material into two pieces. In other words the surface energy is the work done when creating a surface. The surface energy of a single component system is always positive. However, in multicomponent system, due to the interaction between the surface and ITS surroundings the surface energy changes and it can even become negative [19]. The method used to calculate the surface energy of clean Au surfaces and Au surfaces with adsorbates is explained below.

The system under study is represented as a slab (see Fig. 2.3) and has surfaces at the top and bottom. The surface energy is obtained by subtracting the bulk energy from the total energy of the slab [20, 21, 22]. In all calculations we have assumed that the bulk energy of the system is constant for a given thickness. Mathematically above statement can be written as

$$\gamma_{hkl}^{Au} = \frac{E_{slab} - \varepsilon_{bulk} N_{slab}}{A_{tot}} \quad (3.4)$$

which can be rearranged into

$$\frac{E_{slab}}{A_{tot}} = \gamma_{hkl}^{Au} + \frac{\varepsilon_{bulk}}{A_{tot}} N_{slab}, \quad (3.5)$$

where  $\gamma_{hkl}^{Au}$  is the surface energy of clean Au,  $E_{slab}$  is the total energy of the slab,  $\varepsilon_{bulk} N_{slab}$  is the bulk energy, and  $A_{tot}$  the total surface area.

Equation 3.5 corresponds to a straight line whose intercept gives the surface energy of the clean surface and whose slope yields the bulk energy per

atom. Using this approach we have calculated the surface energies for the low indexed surfaces (100), (110), and (111) as well as the high indexed surfaces (210), (310), and (410). These surfaces have been considered because low indexed surfaces are generally stable and they appear in almost all crystalline structures. High indexed surfaces are important because they contain steps, which act as nucleation sites in the process of crystallization.

The free energy of a system containing surface of area  $A$  is

$$G = G_0 + A\gamma \quad (3.6)$$

where  $G_0$  is the free energy of the bulk, and  $\gamma$  the surface energy. The increase in the free energy of the system due to an increase in the surface area by  $dA$  is

$$dG = \gamma dA + Ad\gamma. \quad (3.7)$$

If we assume that the surface energy is independent of the area of the interface then,  $\frac{d\gamma}{dA} = 0$ , which leads to

$$dG = \gamma dA. \quad (3.8)$$

## 3.4 Thermodynamics of Adsorption

### 3.4.1 Adsorbates

Adsorbates are atoms or molecules on a surface, which modify its physical and chemical properties [23, 24]. Apart from modifying the free energy of the system they also modify many other aspects of the dynamics of the surface. Here we will consider only the surface energy, which is a purely thermodynamic effect. The properties of a surface with an adsorbate depend on adsorbate geometry, angular orientation of the adsorbate and the overall structure of surface and adsorbate. Adsorbates can adsorb either physically or chemically to a surface:

1. Physisorption: In this mode adsorbates are bonded to the surface via weak van-der-Waals type forces. Their binding energy is typically comparable to  $kT$ .
2. Chemisorption: Adsorbates in this mode are strongly bonded to the surface e.g, by ionic or covalent bonding. The binding energy in this case is much higher than  $kT$ . This type of bonding is important in the study of surfaces because there is substantial redistribution of electrons between adsorbate and surface. Chemisorption is almost always exothermic.



The rate of adsorption of a molecule onto a surface follows an Arrhenius form

$$R_{ads} = A \exp \left[ -\frac{E_a}{kT} \right] \quad (3.9)$$

where  $E_a$  is the activation energy for adsorption,  $k$  is the Boltzmann constant, and  $A$  is a pre-factor.

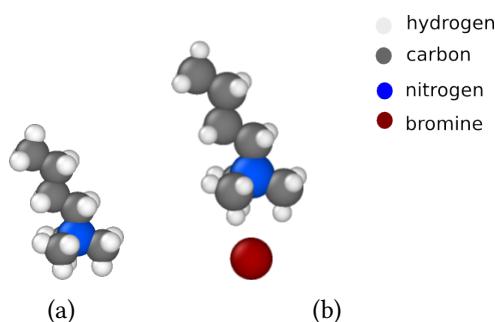


**Figure 3.4:** (a)  $(\text{H}(\text{CH}_2)_4\text{N}(\text{CH}_3)_3^+)$  butyltrimethylammonium and (b)  $(\text{H}(\text{CH}_2)_4\text{N}(\text{CH}_3)_3\text{Br})$  butyltrimethylammonium bromide.

In this work, the adsorption of bromine (Br), butyltrimethylammonium cation  $\text{BTA}^+$ , and butyltrimethylammonium bromide (BTAB) has been studied on (100), (110), (111), and (310) surfaces. We chose these adsorbates for our study because alkyltrimethylammonium bromides ( $\text{C}_n\text{TAB} = \text{C}_n\text{H}_{2n+1}\text{N}(\text{CH}_3)_3\text{Br}$ ) where  $n$  is the chain length, are the most widely used surfactant in seed-mediated growth [25, 26, 8] of gold nanoparticles. We have used a shorter chain length ( $n = 4$ ) in our study to save valuable computational time. The choice of counter ion  $\text{Br}^-$  is motivated by the work from Garg and co-workers [7] who proposed  $\text{Br}^-$  as a suitable candidate because of its moderate binding with the gold surface.

### 3.4.2 Approximations

The thermodynamic environment, in which Au nanorod growth occurs experimentally, is not amenable to direct modeling by DFT due to its complexity. We therefore make a series of approximations as outlined in this section. DFT calculations are done at  $T = 0$  K whereas real time growth occurs at finite temperatures.

Figure 3.5 shows the effect of various thermodynamic parameters on the structure of a surfactant. The Gibbs free energy  $G = H - TS$  of the surfactant comprises both entropy and internal energy. By bringing the surfactant from its reservoir, for example from vacuum or solution, onto the surface the change

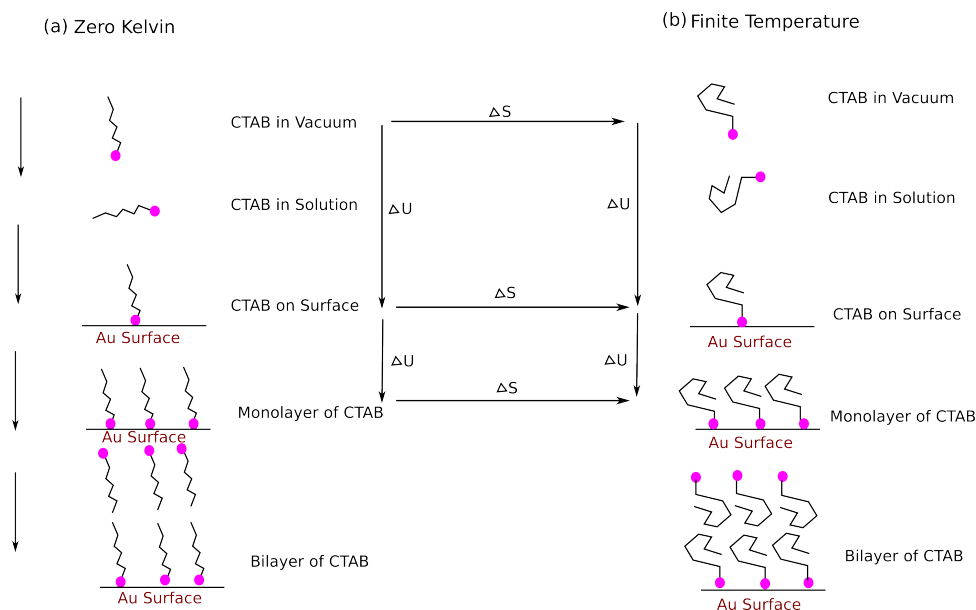


**Figure 3.5:** Schematic visualizing the different thermodynamic contributions that arise along the transition in the state of surfactant as it is adsorbed from reservoir onto the surface at zero K (a) transition in the state of surfactant as it adsorbed from the reservoir(vacuum) onto the surface at some finite temperature (b).

in Gibbs free energy is mainly due to the internal energy. At lower temperatures the entropy is small compared to the internal energy of the surfactant. Solvation effects should also be small compared to the heat of adsorption. In our calculations the chemical potential of all surfactants is measured with respect to the vacuum.

We have used BTAB as a prototype for the surfactant CTAB used experimentally. BTAB has only four carbon atoms in its chain compared to 16 in the case of CTAB. This selection is motivated by the fact that the difference in the adsorption energy for the case of BTAB and CTAB is small [27]. The only major change is due to weak van-der-Waals interactions between adjacent chains.

### 3.4.3 Adsorption Sites

The motivation for doing the adsorption study on low index surfaces (100), (110), and (111) is that these surfaces always appear after nucleation and play a key role in crystal growth. Another advantage is that their DFT computation is quite efficient. High index surfaces, such as (310) are important because of their structure. Step atoms on these surfaces have lower coordination, which makes these surface more reactive. Evidences [28, 1] have been found for the

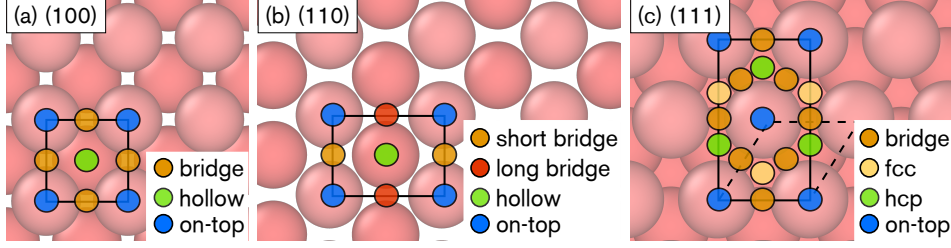


Figure 3.6: Adsorption sites on (100), (110), and (111) FCC surfaces.

presence of high indexed surfaces in gold nanorod growth. Indexed surfaces have lower symmetry and there are many more degrees of freedom for placing adsorbates. Figure 3.6 shows all possible adsorption sites on low index planes of FCC system. It is clear from this figure that there are many possible adsorption sites, for example bridge, hollow, on-top, fcc, and hcp. The high index plane (310) shown in Fig. 4.6 is composed of low index planes. Its terrace has a structure like (100) planes and steps resembles (110) planes.

### 3.5 Coverage

The surface energy of a clean surface is constant if there is no defect formation or reconstruction of the surface. The situation, however, changes with adsorbates on the surface. Adsorbates can form strong covalent, metallic, and ionic type bonds with the substrate. Strong bonds change the electronic structure of the substrate close to the surface. Adsorbates change the free energy of the system. In the case of a crystal this change is orientation dependent, which is also called surface energy anisotropy. The surface energy in the presence of an adsorbate is given by

$$\gamma_{hkl}^{Au+ads} = \gamma_{hkl}^{Au} + \Delta\gamma_{hkl}^{ads}, \quad (3.10)$$

where  $\Delta\gamma_{hkl}^{ads}$  is the Gibbs free energy of adsorption per unit area,  $\gamma_{hkl}^{Au}$  is the surface energy of the clean surface, and  $\Delta\gamma_{hkl}^{ads}$  is the change in the Gibbs free energy per unit area of the system

$$\Delta\gamma_{hkl}^{ads} = \frac{\Delta E_{ads} - \mu}{A_{tot}} \quad (3.11)$$

where  $\Delta E_{ads}$  is the adsorption energy and  $\mu$  is the chemical potential of the adsorbate. It is evident from Eq. (3.11) that the chemical potential and thus the surface energy are dependent on surface coverage. The surface coverage is

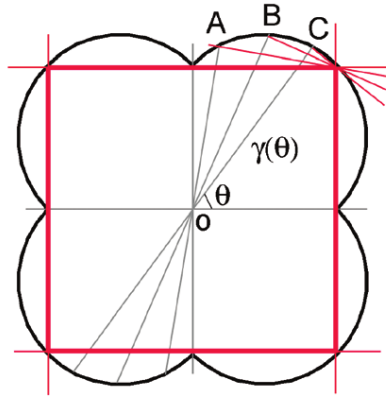


**Figure 3.7:** Polar plot of surface energy  $\gamma(\theta)$  for a square lattice. The radius vectors OA, OB, and OC represents the free energy of a surface plane whose normal lies in that direction. Thus  $OA = \gamma_{100}$ ,  $OB = \gamma_{111}$ , etc. The inner envelope (red line) of all such Wulff planes gives the equilibrium shape of the crystal.

measured as

$$\begin{aligned} \text{adsorbates per surface supercell} &= \frac{\text{number of adsorbate species in supercell}}{\text{number of surface atoms in supercell}} \\ \text{adsorbates per unit area} &= \frac{\text{number of adsorbate species in supercell}}{\text{cross sectional area of supercell}}. \end{aligned}$$

During surfactant assisted crystal growth, surfactants show an affinity towards certain crystal planes. A large negative adsorption energy is a signature of favourable binding to that facet. We saw in the previous section how adsorbates influence the surface free energy. Thus it is possible to change the surface free energy of different facets at different rates, which represents the basic principle of anisotropic growth under a finite driving force. We will, however, see that this is not always the case as there are several other factors which shifts the reaction away from equilibrium.

### 3.6 Equilibrium Shape

The free energy of a system containing an interface of area  $A$  and interfacial free energy  $\gamma$  per unit area is given by

$$G = G_{bulk} + A\gamma \quad (3.12)$$

where  $G_{bulk}$  is the free energy of the bulk and  $\gamma$  is the excess free energy due to broken bonds close to the surface. The number of broken bonds at the surface

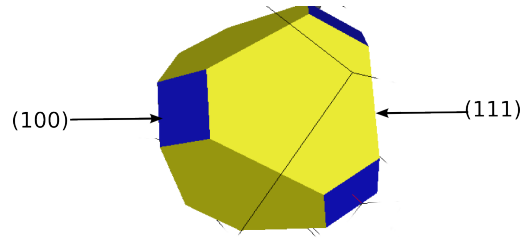


**Figure 3.8:** A truncated cuboctahedral equilibrium shape of an FCC crystal bounded by 111 and 100 facets.

increases as one gradually moves from low to high index planes. A convenient method for plotting the variation of surface energy with surface orientation is to construct the polar plot of surface energies  $\gamma(\theta)$ .

The equilibrium shape of a crystal can be geometrically determined from the polar plot of surface energies as suggested by Wulff [29]. The Wulff construction, which gives the shape with the minimum  $\sum \gamma_{hkl} A_{hkl}$ , provides the equilibrium shape of a crystal based on variations in surface energy as a function of orientation. The steps involved in the construction can be summarized as follow

1. Obtain the polar plot of the surface energy from broken bond theory
2. For every point on the  $\gamma$  surface, a plane is drawn through the point and normal to the radius vector

The equilibrium shape is then simply the inner envelope of all such planes.

Crystals under equilibrium obtain a shape which has lowest surface energy for a given volume. An equilibrium shaped crystal has to satisfy the condition that  $\sum \gamma_{hkl} A_{hkl}$  be minimum, where  $\gamma_{hkl}$  and  $A_{hkl}$  are the interfacial free energy and the area of  $hkl$  planes respectively. Note that the structure obtained from the Wulff construction is different from the condition that  $\sum \gamma_{hkl}$  or  $\sum A_{hkl}$  be minimum individually.

In this thesis work, we have used Wulffmann software, a program [29] developed to obtain the equilibrium shape of a crystal. An example for a crystal obtained in this fashion is shown in Fig. 3.8.

# Chapter 4

## Results and Discussion

### 4.1 Adsorption

#### 4.1.1 Adsorption Sites

In order to study adsorption on any surface it is vital to identify adsorption sites first. Figure 3.6 shows all possible sites for adsorption on low index FCC planes. At maximum coverage, a monolayer is formed. Here we assume that adsorption occurs only on the sites on the surface, not on the top of another adsorbate.

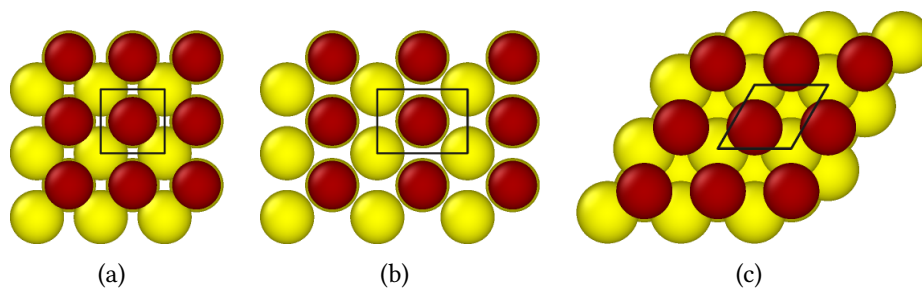
#### 4.1.2 Br on Low Index Au Surfaces

In order to find the energetically most favourable site for Br, Br is manually incorporated at the sites shown in Fig. 3.6 and their adsorption energies are compared. The results are summarized in Table 4.1 which shows that the bridge site is energetically most favourable site. The same approach is taken to find the most stable sites for Br on (110) and (111) surfaces. For the case of (110) surface, bridge site is found most stable and for (111) surface, it is the fcc site.

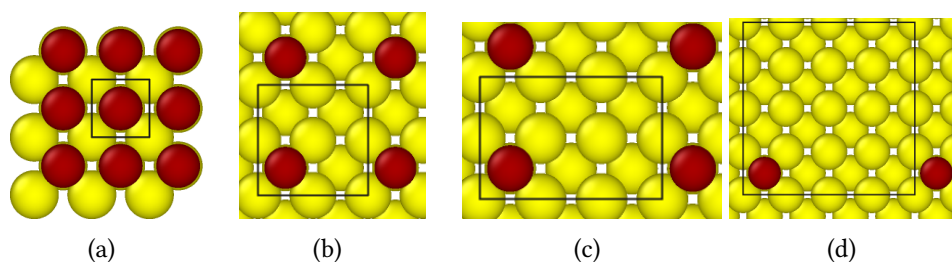
To illustrate the effect of the surface coverage let us consider the adsorption of Br at hollow sites on (100) Au surfaces. The different coverages are represented by size of the supercell. A large supercell, for example  $4 \times 4$  surface unit

Table 4.1: Adsorption energies of Br for various sites on (100) Au surface at full coverage.

Adsorption site	on-top	hollow	bridge
Adsorption energy $E_{ads}$ (eV)	-0.75	-0.99	-1.08



**Figure 4.1:** Br on various FCC Au surfaces.  $1 \times 1$  supercells of (a) (100) (b) (110), and (c) (111) surfaces.



**Figure 4.2:** Br on FCC Au (100) hollow sites at different coverages. (a)  $1 \times 1$  supercell (1 monolayer = 1 adsorbate per substrate atom), (b)  $2 \times 2$  ( $1/4$  monolayer), (c)  $3 \times 2$  ( $1/6$  monolayer), and (d)  $4 \times 4$  ( $1/16$  monolayer coverage).

**Table 4.2:** Adsorption energy of Br on Au (100) surfaces with respect to surface coverage. The surface coverage is expressed in terms of monolayer (ML).

Coverage (ML)	1	$1/2$	$1/4$	$1/6$
Adsorption energy $E_{ads}$ (eV)	-0.02	-0.46	-1.05	-1.09

**Table 4.3:** Adsorption energies of  $\text{BTA}^+$  at various sites on Au (100) surfaces at full coverage.

Adsorption site on (100)	$E_{ads}^{\text{BTA}^+}$
on-top	-1.90
hollow	-1.86
bridge	-1.88

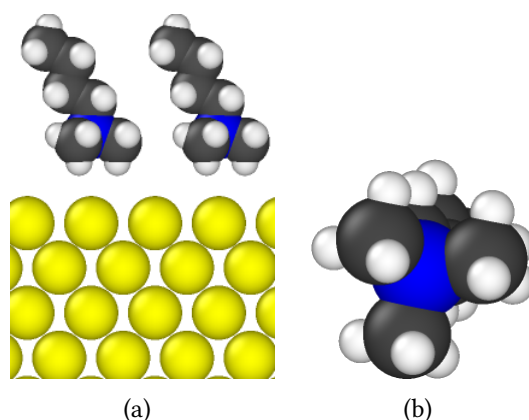


**Figure 4.3:** (a)  $\text{BTA}^+$  cation on the Au (100) surface on-top site. (b) Triangular shape of the base of the  $\text{BTA}^+$  cation. Nitrogen is represented in blue, carbon in grey, and hydrogen in white.

cells, represents very low coverage. From Table 4.2 we can see that the adsorption energy is becoming more negative as we go from high surface coverage to low coverage. Comparing the adsorption energies at coverages of 1/4 ML and 1/6 ML we see that the difference in the adsorption energy is only  $-0.04$  eV. This is an indication that the dilute limit has been reached and there will not be any further change in the adsorption energy at lower coverages.

### 4.1.3 $\text{BTA}^+$ on Low Index Au Surfaces

In the following the position of the  $\text{BTA}^+$  cation is measured with respect to the position of the nitrogen relative to the surface site. The adsorption energies are summarized in Table 4.3. From this table it is evident that the on-top site on the (100) surface is the most favourable site for  $\text{BTA}^+$ . The same approach is taken to find the most stable sites on (110) and (111) surfaces. The on-top site is found to be the most stable site in all cases. This probably due to the electron deficient cation  $\text{BTA}^+$  favouring to sit close to an Au atom.



**Table 4.4:** Adsorption energy of  $\text{BTA}^+$  at full coverage incorporated at the most stable site.

Surface	Adsorption site	Adsorption energy (eV)
(100)	on-top	-1.76
(110)	on-top	-3.36
(111)	on-top	-1.43

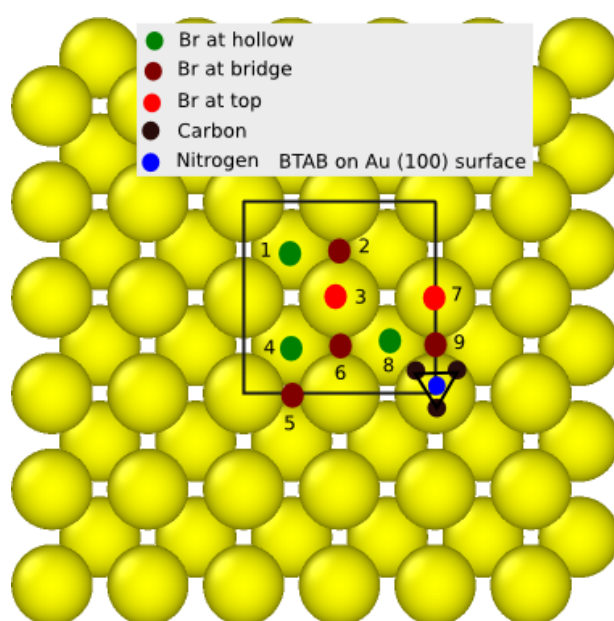


**Figure 4.4:** BTAB surfactant on FCC gold surface (100).  $\text{BTA}^+$  is located at the on-top site in a  $2 \times 2$  supercell and Br at all possible sites in the supercell.

#### 4.1.4 BTAB on Low Index Surfaces

Now that we have found the most stable sites for Br and  $\text{BTA}^+$  on low index surfaces, we continue with the analysis of BTAB on low index surfaces.  $\text{BTA}^+$  is first placed on the on-top site which is the most favourable site for  $\text{BTA}^+$  based on the result from the previous subsection. Br is then placed at all available sites in the supercell see Fig. 4.5. Utilizing the symmetrical structure of  $\text{BTA}^+$  a few sites are excluded from the computation. From Table 4.5 it is evident that the most stable structure of BTAB on Au (100) is with  $\text{BTA}^+$  at the on-top site and Br at the bridge site.

**Table 4.5:** Relative energies of a  $2 \times 2$  supercell of Au (100) surface with one BTAB molecule. The numbers in the first column are the corresponding sites for Br in the supercell as shown in Fig. 4.4.

Site	1	2	3	4	5	6	7	8	9
Energy (eV)	-6.95	-6.90	-6.92	-0.01	-3.01	-6.92	-7.00	0.00	-7.10

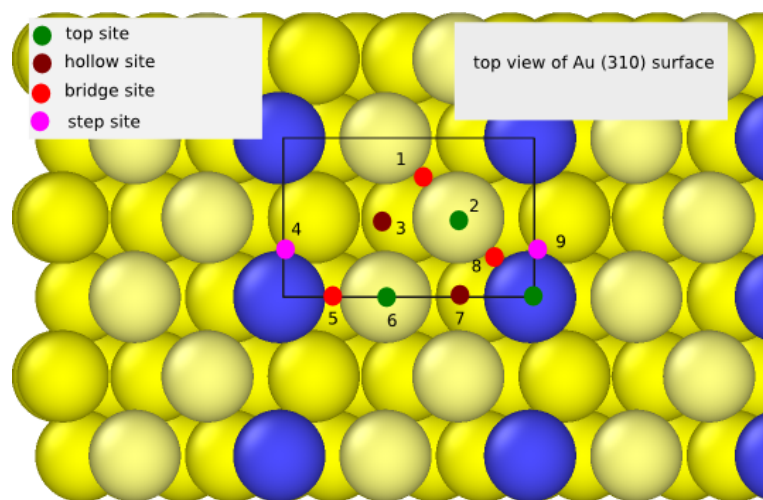


**Figure 4.5:** Adsorption sites on (310) Au surfaces. The supercell contains one primitive unit cell shown by the black rectangle. Atoms in blue are step atoms, light yellow atoms are terrace atoms and dark yellow are bulk atoms. All crystallographically distinct possible adsorption sites are marked with numbers.

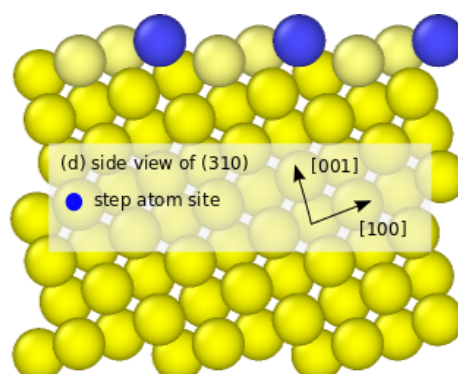


**Figure 4.6:** Side view of Au (310) surface with step atoms highlighted in blue.

**Table 4.6:** Relative energies of a  $1 \times 1$  supercell of Au (310) surface with one Br. The numbers in the first column are the corresponding sites for Br in the supercell as shown in Fig. 4.5.

Site	1	2	3	4	5	6	7	8
Energy (eV)	-0.15	-0.16	-0.09	-0.16	-0.07	-0.08	0.00	-0.15

**Table 4.7:** Relative energy of a  $1 \times 2$  supercell of Au (310) surface with one  $BTA^+$  cation. The numbers in the first column are the corresponding sites for  $BTA^+$  in the supercell as shown in Fig. 4.5.

Site	1	2	3	4	5	6	7	8
Energy (eV)	-0.19	-0.15	0.00	-0.16	-0.20	-0.24	-0.10	-0.03

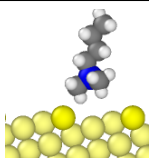
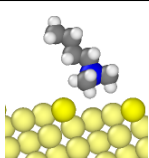
#### 4.1.5 Br on High Index Surface

Along with the low index surfaces, the high index (310) surface is also considered in this study. High index surfaces are chosen because of the presence of surface steps, which provide reactive sites and are seen as nucleation sites during crystal growth. Br is placed at all the sites shown in Fig. 4.5 and the total free energy of the system is calculated. The results shown in Table 4.6 demonstrate that the step sites, indicated by numbers 4 and 9 in Fig. 4.5, are energetically the most favourable sites for Br.

#### 4.1.6 $BTA^+$ on High Index Surface

We use Fig. 4.5 to identify the adsorption sites for  $BTA^+$  on the (310) surface. A supercell of size  $1 \times 2$  is used in the analysis because of the large size of  $BTA^+$ . The results shown in Table 4.7 reveal the most favourable site for  $BTA^+$  on the (310) surface. The most favourable site for  $BTA^+$  is site number 6 as shown in

**Table 4.8:** Two possible orientations of  $BTA^+$  on (310) with respect to the step, which is shown in dark yellow. The adsorption energy is calculated for each geometry and tabulated in the second column.

Orientation		
Adsorption energy (eV)	-2.71	-2.82

**Table 4.9:** Four possible orientations of BTAB on (310) Au surface with respect to the step site, which is shown in dark yellow. These four geometries have been considered based on the orientation of the tail with respect to the step and the position of Br with respect to the tail.

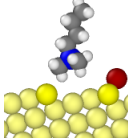
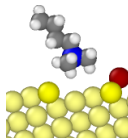
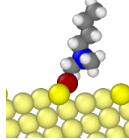
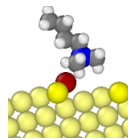
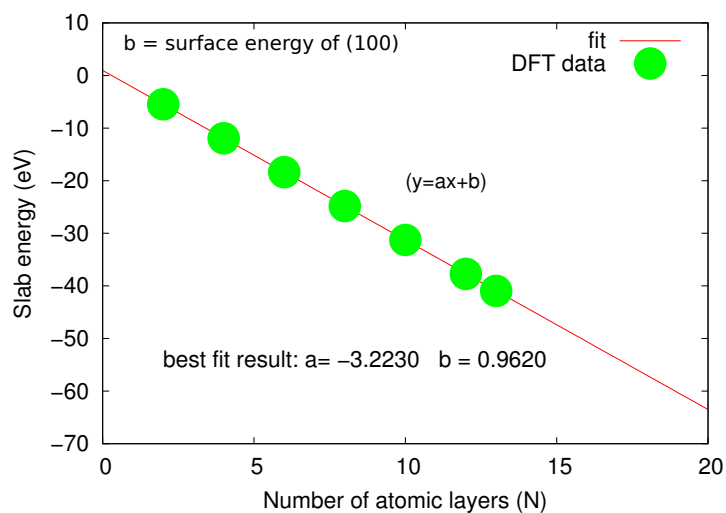
Orientation				
Adsorption energy (eV)	-1.11	-1.23	-1.45	-1.43
$d_{N-Br}$ (Å)	4.98	7.64	4.72	4.94

Fig. 4.5, which is between the two step sites represented by numbers 4 and 9. In next step, we take into account the rotation of  $BTA^+$  with respect to its tail. In one orientation, the tail of  $BTA^+$  is pointing towards the step while it faces in the opposite direction in the second.

The difference in the energy for the above case is approximately 0.1 eV, which is higher than the thermal energy (0.026 eV) at room temperature. This difference in the adsorption energy is due to the position of chain atoms with respect to the step site. The chain atoms in one orientation are closer to the step than the other. It is the interaction between the atoms in the tail of the surfactant and the step atoms, which makes one structure stable than the other.

#### 4.1.7 BTAB on High Index Surface

From the previous subsections on Br and  $BTA^+$  on high index surfaces, we now know the most stable sites for Br and  $BTA^+$  on (310) surface. The most stable site for Br is near the step and for  $BTA^+$  it is on the terrace. Now we find the most stable orientation of  $BTA^+$  with respect to the step site in the presence of Br. The results are summarized in Table 4.9 and reveal the most stable geometry of BTAB on (310) surface. In this configuration  $BTA^+$  and Br sit close to each other.



**Figure 4.7:** Surface energy of FCC gold (100). The abscissa yields the (100) surface energy.

**Table 4.10:** Surface energy of high and low index FCC Au surfaces.

$hkl$ (surface)	$\gamma_{hkl}(J/m^2)$
(100)	0.8881
(110)	0.9984
(111)	0.7333
(210)	1.0215
(310)	0.9396
(410)	1.0106

## 4.2 Surface Energy

### 4.2.1 Surface Energies of Clean Au Surfaces

The surface energy of an  $N$  atomic layer thick clean gold surface can be expressed as described in Sect. 3.3 as

$$\frac{E_{slab}}{A_{total}} = \gamma_{hkl}^{Au} + \frac{\varepsilon_{bulk}}{A_{tot}} N_{slab},$$

where  $E_{slab}$  is the total energy of the slab and  $A_{total}$  is the combined area of top and bottom surfaces. Equation (3.5) corresponds to a straight line whose intercept is the surface energy of the gold surface and the slope is the bulk energy per atom. The surface energy is obtained by fitting as shown in Fig. 4.7.

Using this approach, the surface energies of several gold surfaces have been calculated as tabulated in Table 4.10. It is evident from these data that (111) is the most stable surface whereas for example (110) is energetically less favourable. This result can be explained by the broken bond model. In creating a FCC (110) surface, five bonds per unit cell are broken, whereas there are four in the case of (100) and only three in the case of (111). The (111) surface is a closely packed smooth surface, whereas (110) is an open surface with many undercoordinated atoms.

### 4.2.2 Surface Energies Change due to Adsorption

In this section we study the change in Gibbs free energy of the system due to adsorption of Br, BTA<sup>+</sup>, and BTAB. The total surface energy in the case of adsorption is

$$\gamma_{hkl}^{Au+ads} = \gamma_{hkl}^{Au} + \Delta\gamma_{hkl} \quad (4.1)$$

where  $\Delta\gamma_{hkl}$  is the Gibbs free energy change per unit area,  $\gamma_{hkl}^{Au}$  the surface energy of the clean surfaces, and  $\gamma_{hkl}^{Au+ads}$  is the surface free energy post adsorption.

#### Br Adsorption

Figure 4.8 shows the change in the Gibbs free energies of various gold surfaces in the presence of Br. The change in the energy density depends on the chemical potential of Br, which represents the potential of the reservoir. Here we reference  $\mu$  with respect to the Br dimer in vacuum, which sets the zero of the energy scale,  $\mu = E_{dimer} + \Delta\mu$ . It is clear from Fig. 4.8 that the change in the free energy according to Eq. (4.1) is different for different surfaces.

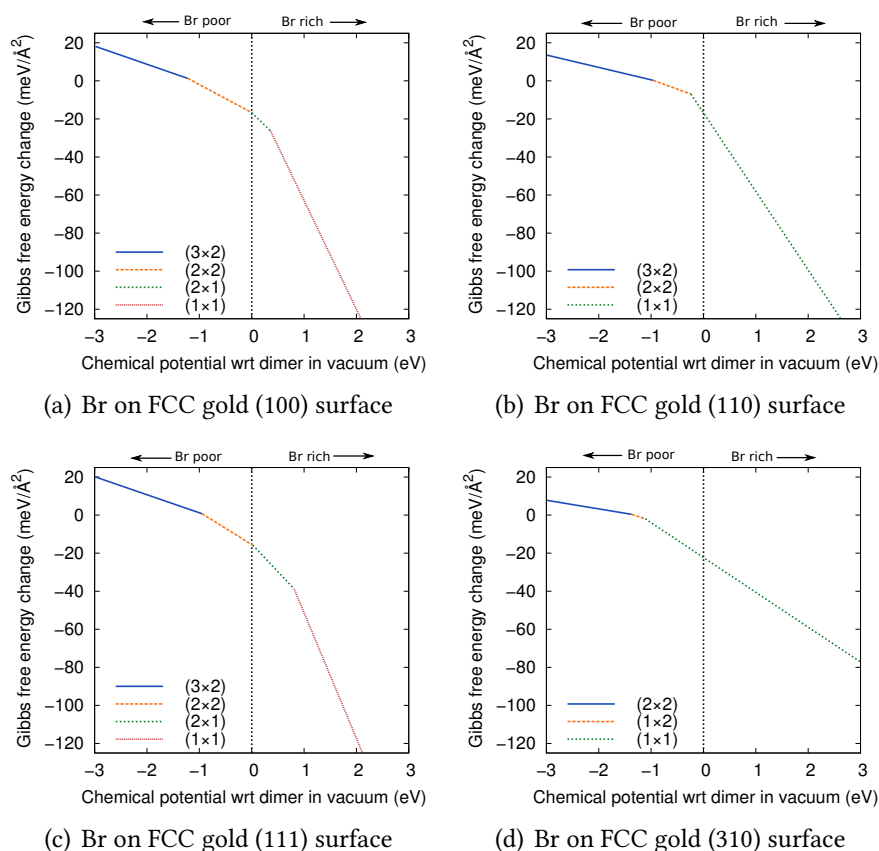


**Figure 4.8:** Gibbs free energy change of Au surfaces with Br as adsorbate at different surface coverages. The chemical potential of Br is measured with respect to the dimer in vacuum. Different line styles correspond to different surface cells and thus different coverages, for example  $1 \times 1$  represents the highest coverage.

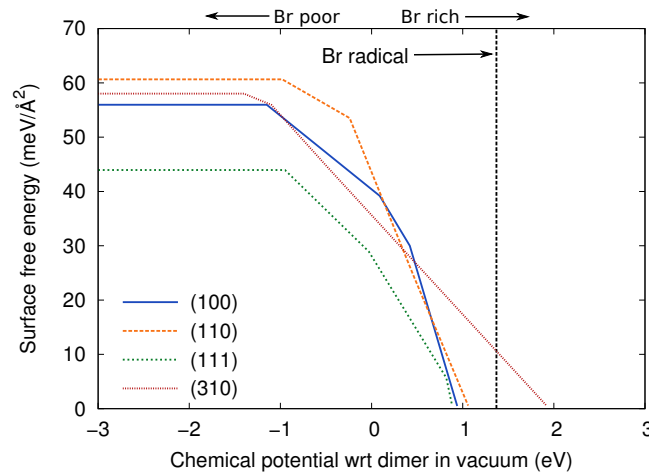


**Figure 4.9:** Variation in the surface free energies of various FCC gold surfaces in the presence of Br. The chemical potential of Br is measured with respect to the dimer in vacuum. Different line styles represent different surfaces.

By combining the data from Fig. 4.9 with the values for the energy density of clean Au surfaces from Table 4.11 we obtain the total surface free energy from Eq. (4.2). Figure 4.10 gives information about the relative stability of surfaces. On the extreme left of the plot in Fig. 4.10, which represents clean surfaces shown as flat lines, we can see that the (111) surface is by far the most stable. However, with the increase in the chemical potential, the (110) surface transforms into a more stable state and it even equals the most stable surface (111) close to  $\Delta\mu = 0$ . Note that the data in Fig. 4.10 implies that the crystal becomes unstable ( $\gamma < 0$ ) with respect to surface formation already at  $\Delta\mu < 1$  eV below the Br radical.

### BTA<sup>+</sup> Adsorption

Figure 4.11 shows the change in the Gibbs free energies of various gold surfaces due to the presence of BTA<sup>+</sup>. The change in the energy density has the same dependence on the chemical potential of BTA<sup>+</sup> as explained in the previous subsection for the case of Br. The main difference in the adsorption of BTA<sup>+</sup> and Br on these surfaces is the large change in the free energy of (110) with BTA<sup>+</sup>. This is due to the large adsorption energy of BTA<sup>+</sup> on the (110) surface as shown in Table 4.4.

The total surface free energies with respect to the chemical potential of BTA<sup>+</sup> have been calculated the same way as explained for the case of Br. We can see in Fig. 4.11 that the surface energy of (110) is decreasing much faster than for the other surfaces. This is because of the large change in the Gibbs free



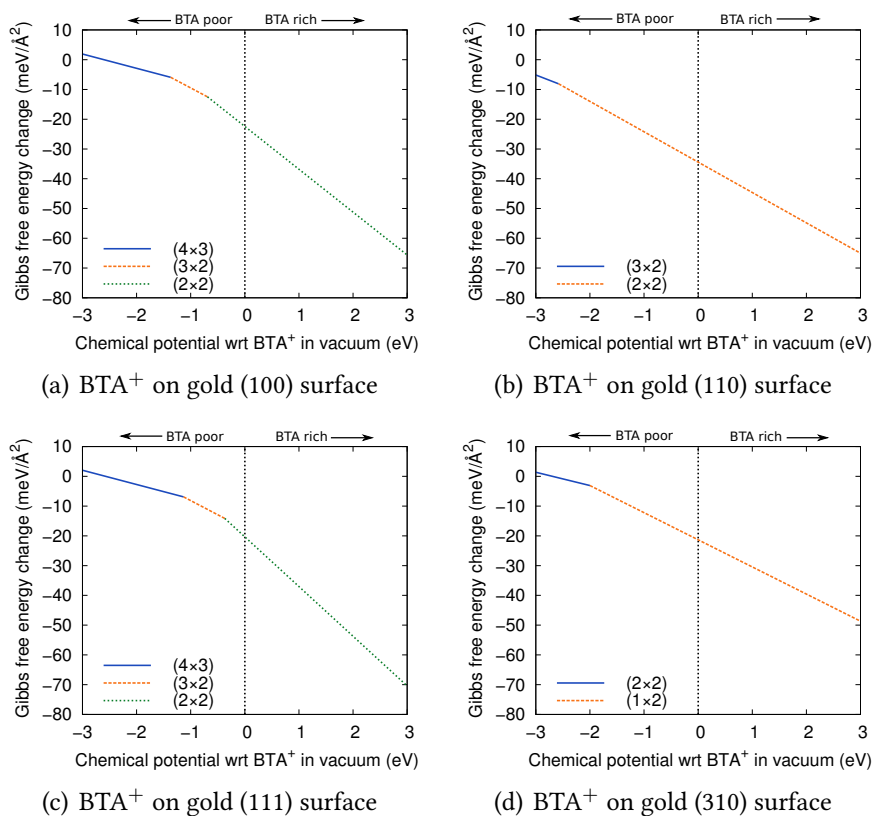


**Figure 4.10:** Gibbs free energy change of Au surfaces with BTA<sup>+</sup> as adsorbate at different surface coverages. The chemical potential of BTA<sup>+</sup> is measured with respect to BTA<sup>+</sup> in vacuum. Different line styles represent different surface cells, for example 1 × 2 represents the highest coverage.

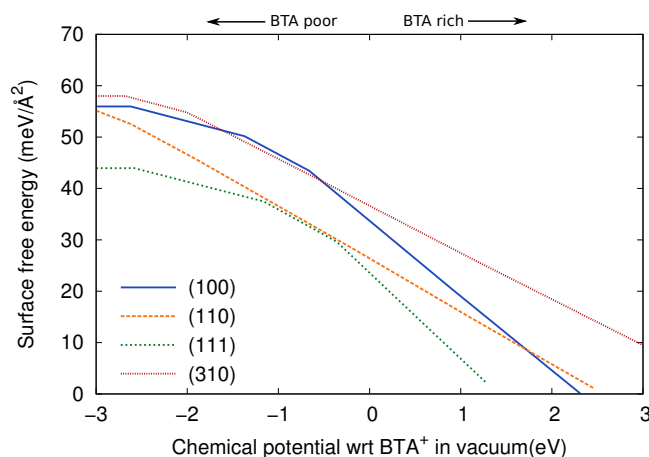


**Figure 4.11:** Variation of the surface free energies of various FCC gold surfaces in the presence of  $\text{BTA}^+$ . The chemical potential is measured with respect to  $\text{BTA}^+$  in vacuum. Different line styles represent different surfaces.

energy of (110) surface after adsorption of  $\text{BTA}^+$ . This is an important result because (110) lowers its surface energy at a much faster rate and becomes as stable as (111) at lower chemical potential compared to for example Br.

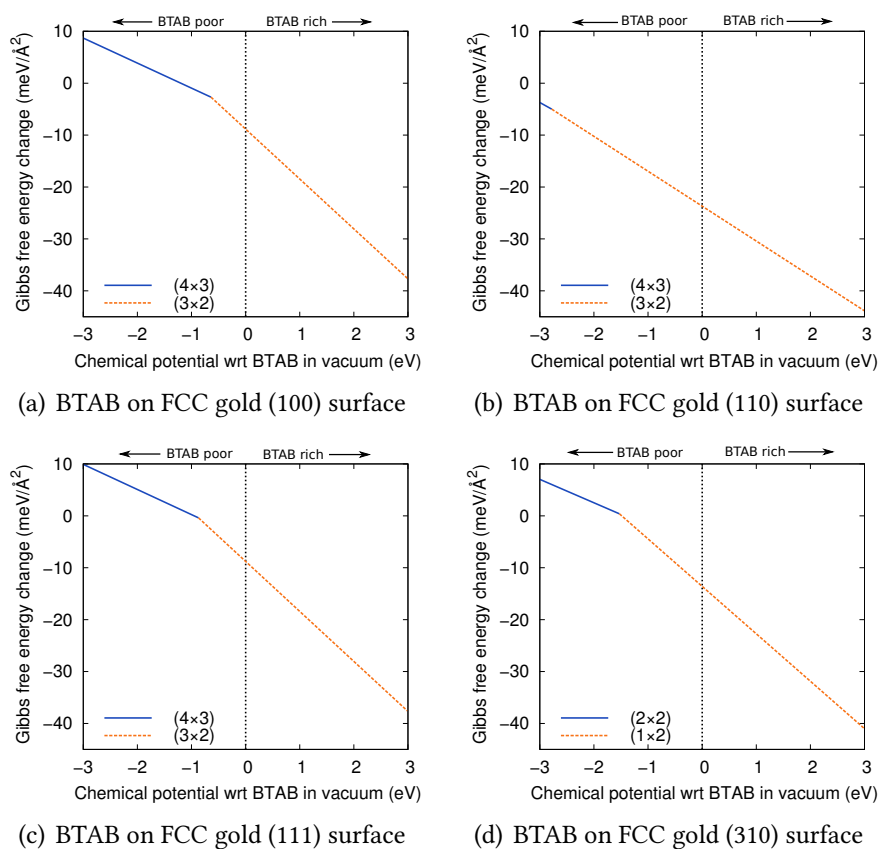
### BTAB Adsorption

Figure 4.14 shows the transition in the stability of various FCC gold surfaces. Surfaces, which are not so energetically favourable in the clean state, for example (110), become increasingly stable when the chemical environment is changed. The effect of BTAB on the high energy planes is evident in Fig. 4.14, where one can see that (110) and (111) have equal surface energy at a chemical potential  $-1$  eV. Note that the (110) surface transforms into a thermodynamically stable plane under the influence of BTAB.

## 4.3 Equilibrium Crystal Shape

We have used the Wulff construction technique[29] to determine the minimum energy crystal shape see section (3.6). The input quantities are the point group symmetry of the crystal and the surface energies of different facets. The space group symmetry used to determine the shape of cubic crystals is  $Fm\bar{3}m$  and the surface energies are taken from section (4.2).

Figure 4.15 shows the variation of the total surface free energies with the chemical potential of Br and shapes of the crystal determined at different chemical potentials. It is evident from Fig. 4.15 that the morphology of the crystal is



**Figure 4.12:** Gibbs free energy change of Au surfaces with BTAB as adsorbate at different surface coverages. The chemical potential of BTAB is measured with respect to BTAB in vacuum. Different line styles represent different cells, for example  $1 \times 2$  represents the highest coverage.

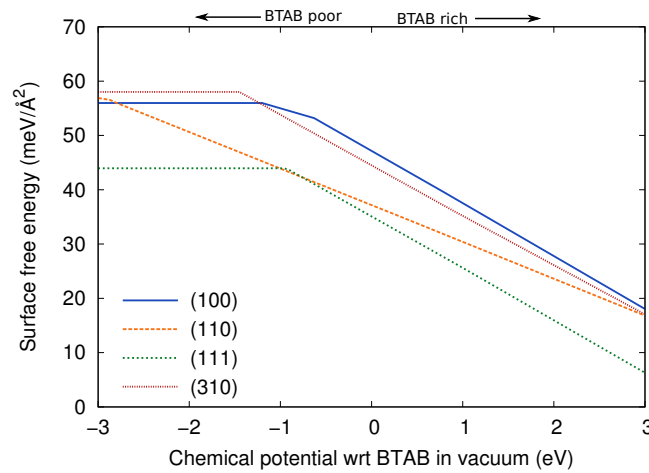
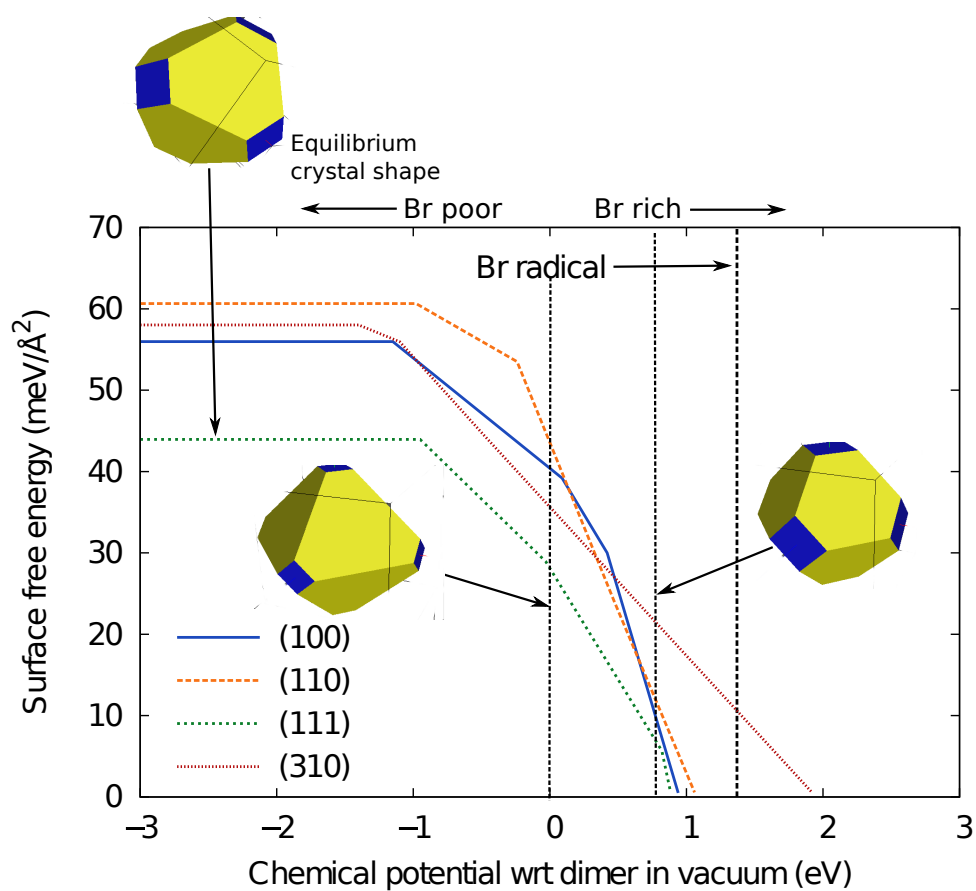


**Figure 4.13:** Variation of the surface free energies of various FCC gold surfaces in the presence of BTAB. The chemical potential is measured with respect to BTAB in vacuum. Different line styles represent different surfaces.

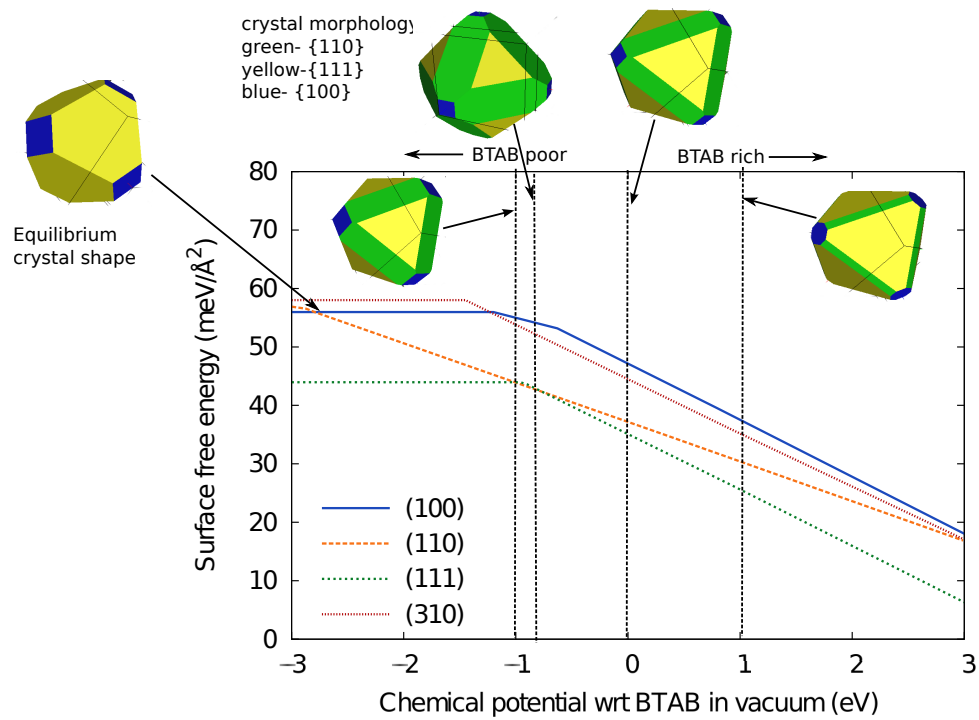
changing with the variation in the surface energy of the surfaces. One can see this effect by looking at the morphology at chemical potentials 0 eV and 0.8 eV. Surfaces which appear in the Wulff shape are thermodynamically stable. Surface (110) is not seen in the morphology, which is because this surface has a significantly higher surface energy than either (111) or (100).

Figure 4.16 shows the variation of the surface free energies of FCC Au with respect to the chemical potential of BTAB. It also shows the morphologies of the crystal at different surface energies. We can clearly see the morphology changing with the surface energies of the surfaces. Facets which are not present in the equilibrium shape, for example (110) appears later when the surface free energy is lowered. For example one can clearly see how (110) grows in size as the chemical potential is changed from -1 eV to  $-0.8$  eV.

These results clarify the effect of the chemical environment on the morphology of the crystal. Certain facets, e.g. 110 appear and grow in size as they are stabilized in the chemical environment. Thermodynamic stability of a particular plane is determined by whether that plane appears on the Wulff shape or not.



**Figure 4.14:** Wulff shape of FCC Au crystal with Br as surfactant. Crystal is bounded by surfaces, (111) in yellow, (100) in blue. Equilibrium shape is also displayed which is calculated from the surface energies of clean Au surfaces.



**Figure 4.15:** Wulff shape of FCC Au crystal with BTAB as the stabilizer. Crystal is bounded by surfaces, (111) in yellow, (100) in blue, and (110) in green. The Equilibrium shape calculated from the surface energies of clean Au surfaces is shown on the far left.



# Chapter 5

## Discussion and Conclusion

### 5.1 Template Assisted Growth

Electrochemical deposition in templates and solution based seed mediated growth are two key methods for the synthesis of anisotropic crystals. Solution-based methods requires precise tuning of nucleation and growth steps to achieve the desired morphology due to complexity of the growth environment . Nanoparticle growth is basically a two step process including nucleation and subsequent growth of nuclei into crystal. Crystal nucleation in solution is largely controlled by thermodynamics. Their shape is dictated by the surface energy anisotropy which is dominant on that scale. Seed crystals aggregate and then break into individual particle multiple times until they reach a critical size which is thermodynamically stable and from where it continues to grow.

The growth mechanism of gold nanorods, a template assisted growth as suggested by Murphy *et al.* [2, 6], where a rod like template (bilayer surfactant structure) is considered as the main driving force for the nanorod formation, which is a case of heterogeneous nucleation. This mechanism, however, is questioned by Garg *et al.* [7] as they showed that nanorod growth is possible even without any template formation in the solution. They also argued that if the micellar template is indeed the reason for nanorod formation, one should not obtain Au nanorods at high yield when CTAB concentration is below its cmc value. Thus the aforementioned arguments clearly indicate that nanorods are not entirely a product of just a template.

#### 5.1.1 Chemical Potential

The thermodynamic environment, in which Au nanorod growth occurs, cannot be reproduced by DFT due to its complexity. It is, however, possible to study the nanorod growth by making a series of well approximations. These



approximations are motivated by the consideration of the magnitude of different contributions as shown in Fig. 5.1. The set of approximations, which we have made in this study are as follow. Entropic contributions and solvation effects have been neglected. We have used BTAB as a prototype for the surfactant CTAB by ignoring weak van-der-Waals interaction.

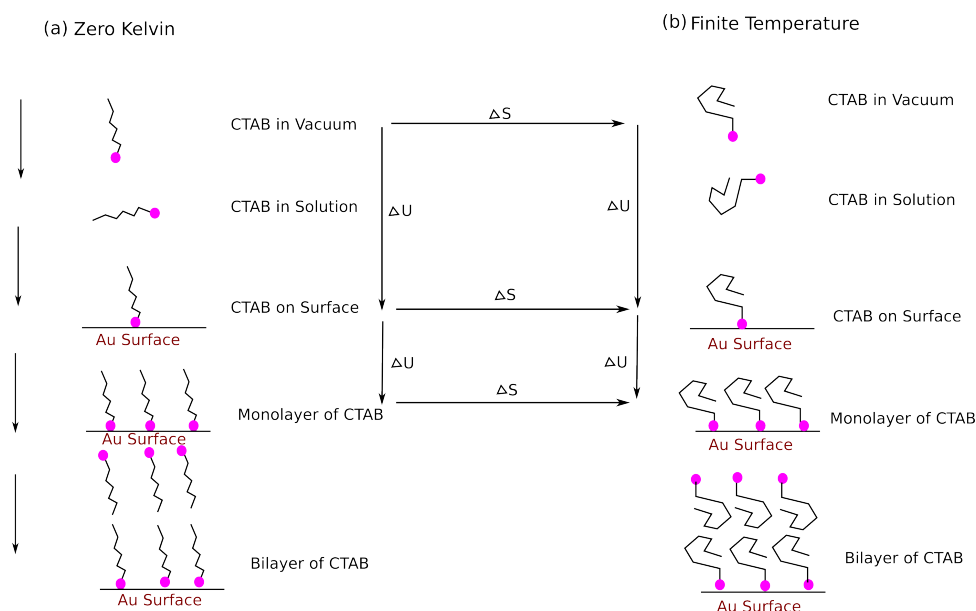


**Figure 5.1:** Schematic visualizing the different thermodynamic contributions that arise along the transition in the state of surfactant as it is adsorbed from reservoir onto the surface at zero temperature (a) transition in the state of surfactant as it adsorbed from the reservoir (vacuum) onto the surface at some finite temperature (b).

The schematic Fig. 5.1 shows the major thermodynamic parameters. The Gibbs free energy  $G = H - TS$  of the system comprises both the entropy and internal energy. Thus by bringing the surfactant from its reservoir (vacuum, solution, etc.) onto the surface, the change in Gibbs free energy is mainly due to its internal energy. At lower temperature the associated entropy term is small compared to the internal energy of the surfactant. Solvation effects are small compared to the heat of adsorption.

### 5.1.2 Anisotropic Shapes and Symmetry Breaking

Anisotropic crystal growth (see Fig. 5.2) cannot be explained by thermodynamics alone. The rate at which monomer crystal units attach to facets and move on these surfaces dictates the non-equilibrium morphology. The rate at

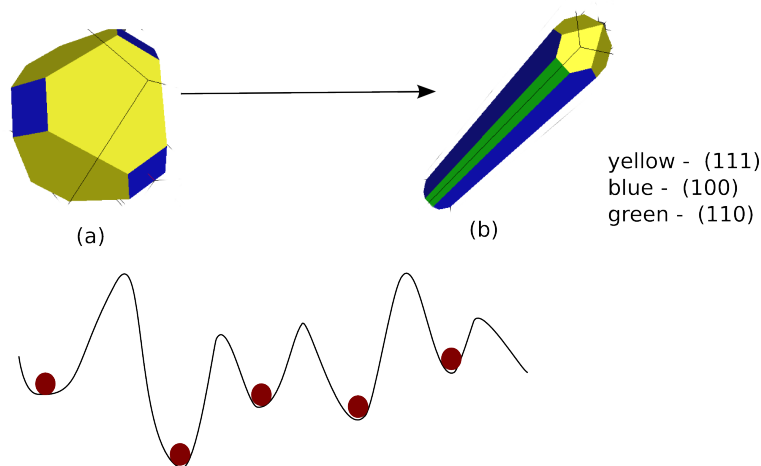


**Figure 5.2:** Growth of gold crystal under finite driving force. Equilibrium shape (a) is denoted as cubo-octahedral while the final shape (b) is in the form of a rod.

which these units migrate on growing facets in turn depends on the energy landscape of the surface. Under a finite driving force two limiting cases can be distinguished as the morphology is controlled by either the adsorption or the surface diffusion rate. The kinetic control hypothesis has been one of the most successful in describing the non-equilibrium morphology of crystals. The main criterion to achieve kinetic control is that the reaction should proceed away from equilibrium. The deviation from equilibrium is rationalized by the change in free energy of crystal facets during the reaction. Figure 5.2 is a good example of kinetically controlled crystal growth where the addition of monomer units to the facets is much slower because of several activation barriers in its migration path. Under such conditions, the end product assumes a shape that deviates from the thermodynamically favoured equilibrium shape.

Under kinetically controlled growth of crystals it is possible to get a variety of crystal morphologies. This can be accomplished by causing the difference in surface energies of different planes by selective adsorption of surfactants on different facets. There are, however, few bewildering morphologies of crystals which cannot be explained entirely based on thermodynamics or kinetics [30].

The growth of an equilibrium shaped cubo-octahedral crystal into a nanorod is an example of a symmetry breaking phenomenon. In the case of symmetry breaking growth is favoured along one out of many symmetry equivalent directions. This class of growth is perhaps instigated by surfactants, for example by oriented attachment of surfactants on crystal facet or by using surfactants as a soft template for the directed growth. Surfactants could amplify the growth rate on a certain facet, those facet grow much faster compare to other facet

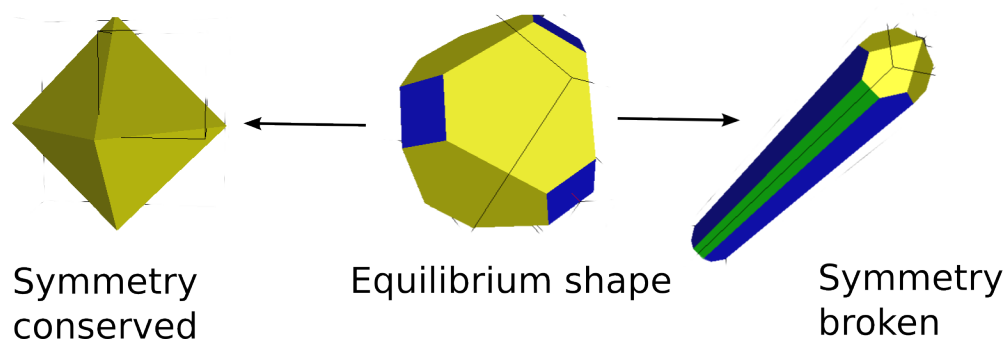


**Figure 5.3:** Representation of growth morphologies in which symmetry is not broken (left) and with broken symmetry (right). The equilibrium shape of crystal is cuboctahedral while the final shape is in the form of a rod when the symmetry is broken and prism shaped when symmetry is conserved.

which leads to the formation of one dimensional structures as shown in Fig. 5.3.

## 5.2 Conclusion

In this thesis work we studied the thermodynamics of growth of gold nanoparticles. We considered (100), (110), (111), and (310) facets, which was motivated by high-resolution transmission electron microscope [31] images indicating that the nanoparticles are bound by the (100), (110), and (111) facets. The equilibrium shape of gold crystals obtained by combining density functional theory calculations and the Wulff construction method was found as cuboctahedral in agreement with the literature [30]. This result is a demonstration that nucleation of any crystal is thermodynamically guided by the predominance of the surface energy term, which dictates the stability and energy of the nucleus. However, growth of the crystal cannot be described by thermodynamics alone.

We have also shown that adsorption of surfactants, specifically Br, and BTAB leads to a considerable reduction of the surface energies. Density functional theory calculations of the interaction of BTAB on gold nanoparticle with several facets shows that the binding of BTAB with (110) is energetically much favourable compared to other low index planes (100), and (111). This leads to a marked reduction of the surface energy of (110) surface with respect to (111) which is by far the most stable surface in the absence of surfactants. This might lead to oriented attachment of BTAB adsorbates on (110) and inhibit growth of this facet.

The Gibbs free energy change of an interface upon adsorption is dependent

on the chemical environment. It depends on the chemical potential of the reservoir. We have been able to show that by changing the chemical potential, it is possible to modulate relative surface energies of interfaces and thus a wide range of morphology is possible. Furthermore, the thermodynamic stability of specific crystal plane determines whether that plane appears on the Wulff shape or not.



# Bibliography

- [1] Grochola, G., Snook, I. K. & Russo, S. P. Computational modeling of nanorod growth. *J. Chem. Phys.* **127** (2007).
- [2] Murphy, C. J. Anisotropic metal nanoparticles: Synthesis, assembly, and optical applications. *J. Phys. Chem. B* **109**, 13857–13870 (2005).
- [3] Jana, N. R. Wet chemical synthesis of high aspect ratio cylindrical gold nanorods. *J. Phys. Chem.* **105**, 4065–4067 (2001).
- [4] Jain, T. *Gold Nanorods Electronics and Self-Assembly*. Ph.D. thesis, University of Copenhagen, Denmark (2012).
- [5] Xiao, J. & Qi, L. Surfactant-assisted, shape-controlled synthesis of gold nanocrystals. *Nanoscale* **3**, 1383–1386 (2011).
- [6] B., N. Evidence for bilayer assembly of cationic surfactants on the surface of gold nanorods. *Langmuir* **17**, 6368–6374 (2001).
- [7] Garg, N., Scholl, C., Mohanty, A. & Jin, R. The role of bromide ions in seeding growth of au nanorods. *Langmuir* **26**, 10271–10276 (2010).
- [8] Liu, M. & Guyot-Sionnest, P. Mechanism of silver(i)-assisted growth of gold nanorods and bipyramids. *J. Phys. Chem. B* **109**, 22192–22200 (2005).
- [9] Park, K. Growth mechanism of gold nanorods. *Chem. Mater.* **25**, 555–563 (2013).
- [10] Sholl, D. S. & Steckel, J. A. *Density Functional Theory* (Wiley, 2009).
- [11] Kresse, G. & Hafner, J. *Phys. Rev. B* **47**, 558 (1993).
- [12] Nightingale, M. P. Quantum monte carlo methods in physics and chemistry. *Mathematical AND Physical Sciences* **525** (1999).
- [13] Hohenberg, P. & Kohn, W. Inhomogeneous electron gas. *Phys. Rev. B* **136** (1964).

## BIBLIOGRAPHY

---

- [14] Kohn, W. & Sham, L. J. Self-consistent equations including exchange and correlation effects. *Phys. Rev.* **140** (1965).
- [15] Perdew, J. P., Burke, K. & Ernzerhof, M. *Phys. Rev. Lett.* **77**, 3865 (1996).
- [16] Blöchl, P. E. *Phys. Rev. B* **50**, 17953 (1994).
- [17] URL <https://wiki.fysik.dtu.dk/ase/ase/ase.html>.
- [18] Stukowski, A. URL <http://www.ovito.org/>.
- [19] Mathur, A., Sharma, P. & Cammarata, R. C. Negative surface energy – clearing up confusion. *Nature Mater.* **4**, 186 (2005).
- [20] Boettger, J. C. Persistent quantum-size effect in aluminum films up to twelve atoms thick. *Phys. Rev. B* **53**, 133–137 (1996).
- [21] Fiolhais, C., Almeida, L. M. & Henriques, C. Extraction of aluminium surface energies from slab calculations: perturbative and non-perturbative approaches. *Prog. Surf. Sci.* **74**, 209–217 (2003).
- [22] Fiorentini, V. & Methfessel, M. Extracting convergent surface energies from slab calculations. *J. Phys* **8**, 6525–6529 (1996).
- [23] Methfessel, M., Hennig, D. & Scheffler, M. Trends of the surface relaxations, surface energies, and work functions of the 4d transition metals. *Phys. Rev. B* **46**, 4816–4829 (1992).
- [24] Scheffler, M. & Stampfl, C. *Theory of Adsorption on Metal Substrates* (2000).
- [25] Sau, T. K. & Murphy, J. Role of ions in the colloidal synthesis of gold nanowires. *Phil. Mag.* **87**, 2143–2158 (2007).
- [26] Si, S. The critical role of the bromide counterion. *Chem. Phys. Chem.* **13**, 193–202 (2012).
- [27] Crawford, R. *Gold Nanorods – The Physics of Anisotropic Crystal Growth*. Master’s thesis, University of Strathclyde (2013).
- [28] Carbo-Argibay, E. & Perez-Juste, J. The crystalline structure of gold nanorods revisited: Evidence for higher-index lateral facets. *Angew. Chem. Int. Ed.* **49**, 9397–9400 (2010).
- [29] Roosen, A. R., McCormack, R. P. & Carter, W. C. Wulffman: A tool for the calculation and display of crystal shapes. *Comp. Mater. Sci.* **11**, 16–26 (1998).

- [30] Viswanath, B., Kundu, P., Halder, A. & Ravishankar, N. Mechanistic aspects of shape selection and symmetry breaking during nanostructure growth by wet chemical methods. *J. Phys. Chem.* **113**, 16866–16883 (2009).
- [31] Johnson, C. J., Dujardin, E., Davis, S. A., Murphy, C. J. & Mann, S. Growth and form of gold nanorods prepared by seed-mediated, surfactant-directed synthesis. *J. Mater. Chem.* **12**, 1765–1770 (2002).